

pubs.acs.org/acscatalysis Research Article

# Switchable Product Selectivity in Diazoalkane Coupling Catalyzed by a Two-Coordinate Cobalt Complex

Yuyang Dong, Michael I. Lipschutz, Ryan J. Witzke, Julien A. Panetier, and T. Don Tilley\*



Cite This: ACS Catal. 2021, 11, 11160–11170



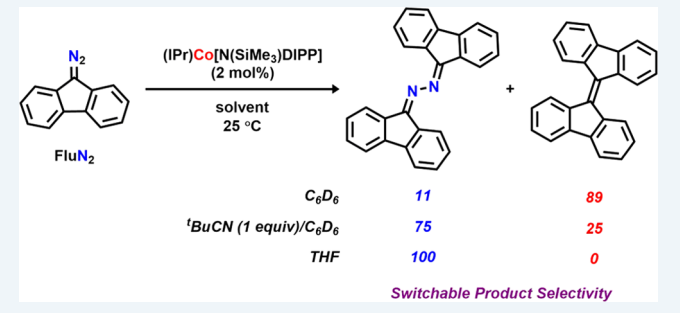
**ACCESS** 

III Metrics & More

Article Recommendations

Supporting Information

**ABSTRACT:** The low-coordinate monovalent cobalt complex (IPr)Co[N(SiMe<sub>3</sub>)DIPP] [2, IPr = 1,3-bis(2,6-diisopropylphenyl)-imidazol-2-ylidene; DIPP = 2,6-diisopropylphenyl], supported by bulky amide and N-heterocyclic carbene (NHC) ligands and its 9-diazofluorene (FluN<sub>2</sub>) adduct (IPr)Co[N(SiMe<sub>3</sub>)DIPP](FluN<sub>2</sub>) (3) are described. Complex 3 was characterized as possessing a high-spin divalent cobalt center antiferromagnetically coupled to a ligand-based radical, resulting in an overall triplet spin ground state (S = 1). Both 2 and 3 are catalyst precursors for the homocoupling of FluN<sub>2</sub> in benzene under ambient conditions to produce 1,2-di(9*H*-fluoren-9-ylidene)hydrazine (8) and 9,9'-bifluorenylidene



(9) in a ratio of 1:8.1. A switch in product selectivity was observed for the reaction in the polar solvent tetrahydrofuran (THF), or in the presence of exogenous good L-type ligands such as *tert*-butylnitrile, to generate the corresponding hydrazine 8 as the major product. A mechanistic study was carried out to rationalize the observed product distributions. The reaction exhibits first-order rate dependence on both the FluN<sub>2</sub> and cobalt catalyst (2) concentrations (monitored by  $^{1}$ H NMR spectroscopy), and 3 was identified as the catalytic resting state. Theoretical calculations were carried out to simulate the production of hydrazine 8 and olefin 9. The result predicted turnover frequencies (TOFs) of  $4.6 \times 10^{-7}$  and  $2.3 \times 10^{-6}$  s<sup>-1</sup> for the generation of 8 and 9 in benzene, respectively, in good agreement with the experimentally observed product ratio. Modeling the reaction in media with higher polarity such as THF resulted in a more favorable kinetic barrier toward the formation of hydrazine 8 due to the stabilization of the more polar C–N bond-forming transition state (8, TOF =  $2.6 \times 10^{-5}$  s<sup>-1</sup> vs 9, TOF =  $6.4 \times 10^{-6}$  s<sup>-1</sup>, in THF). Moreover, simulation of the potential energy surface with a coordinated L-type donor, such as acetonitrile, suggests that the selectivity switch could also result from a modified ligand field, rendering diazoalkane adduct 3 more nucleophilic and lowering the barrier of rate-limiting C–N bond formation to give hydrazine 8.

KEYWORDS: low-coordinate, switchable selectivity, diazoalkane coupling, cobalt, mechanistic study

## 1. INTRODUCTION

Product selectivity is a critical property that defines the utility of a catalyst, and it is a primary consideration in the design of new catalytic processes. <sup>1-6</sup> Thus, an important aspect of catalyst discovery concerns the use of mechanistic information in tuning the reactivity of key intermediates to favor the generation of the desired product over possible side reactions. While the exclusive formation of a given product usually defines the effectiveness of a chemical transformation, the switchability of reaction pathways between different outcomes, depending on conditions such as exogenous additives, reaction temperature, irradiation wavelengths, and solvent identity, has attracted significant interest. <sup>5-11</sup> The prospect of obtaining different products from the same set of reactants and catalysts by simply changing reaction conditions suggests new directions for practical applications of catalysis in chemistry and chemical engineering.

Among the various possibilities for enabling switchable selectivity with transition metal catalysts, changes in the

solvent are relatively easy to employ since the reaction medium greatly influences reactant solubility and can profoundly impact the energetics of alternative reaction pathways.<sup>6,7</sup> Importantly, coordinating solvents may bind to catalytic metal centers, resulting in different coordination spheres that differ substantially in steric and electronic properties.<sup>12,13</sup> These effects are well-known in transition metal-catalyzed cross-coupling reactions,<sup>6</sup> as in the switchable activation of Clvs OTf- groups in Suzuki couplings.<sup>14–16</sup>

Most reports of switchable catalytic selectivity involve second- and third-row late transition metal centers, where two-electron processes dominate the reaction mecha-

Received: June 29, 2021 Revised: August 3, 2021



#### Scheme 1

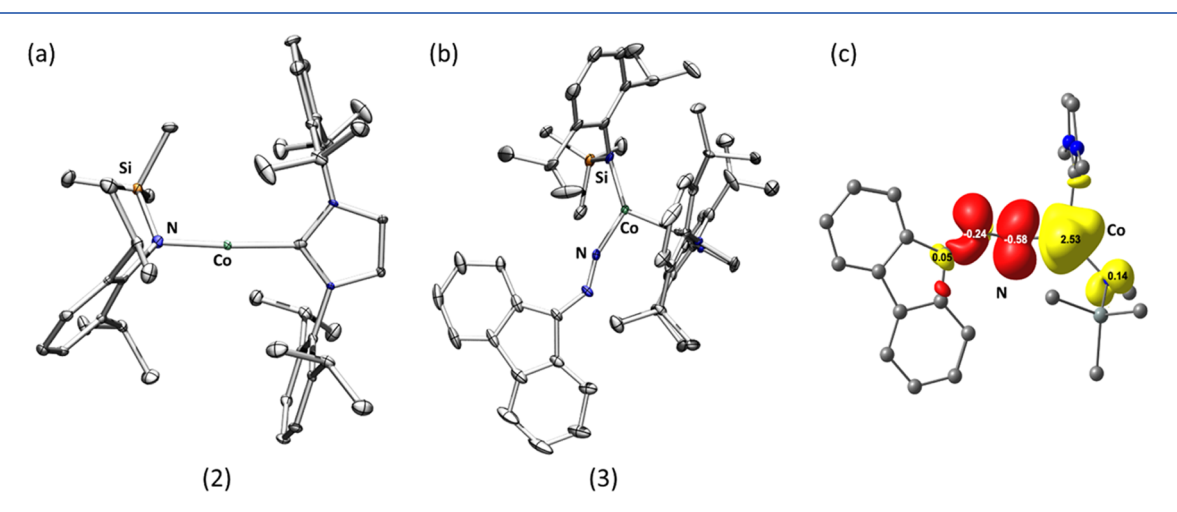


Figure 1. Solid-state molecular structure for (a) (IPr)Co[N(SiMe<sub>3</sub>)DIPP] (2) and (b) (IPr)Co[N(SiMe<sub>3</sub>)DIPP](FluN<sub>2</sub>) (3) with thermal ellipsoids at 50% probability level. Color scheme: Co, aquamarine; N, blue; C, gray; Si, orange. (c) Spin density plot of 3 derived from density functional theory (DFT) calculations  $(\omega B97X-D/BS1)^{47}$  indicating a high-spin divalent cobalt center (S=3/2) antiferromagnetically coupled to a ligand-based radical (S=-1/2), yielding an overall triplet spin ground state  $(S=1)^{39,46}$ 

nism. 6,14–18 First-row metal complexes are less well-studied in this regard, probably due to their distinct chemical properties such as (1) the high-spin electronic configurations associated with the small ligand field splitting in the 3d manifold, (2) facile spin-state changes resulting from perturbations to the ligand field, and (3) reaction patterns dominated by the single-electron chemistry often associated with base metals. Thus, studies of switchable reaction selectivity for base metal catalysts can provide meaningful guidance for the future design of versatile transformations.

Previous work from this laboratory demonstrated the high reactivity and productive catalysis for two-coordinate complexes of 3d metals in hydrosilylation, <sup>25</sup> Kumada coupling, <sup>26</sup> and alkyne trimerization. <sup>27</sup> Here, we present the synthesis and characterization of a low-valent, two-coordinate cobalt complex, as well as its diazoalkane adduct, supported by bulky amido and N-heterocyclic carbene ligands. The electronic structures of these complexes were studied, and

their ability to catalyze the coupling of a diazoalkane is described. This coupling can lead to primarily alkene or hydrazine generation, and the catalytic selectivity can be altered by tuning solvent properties or by adding exogenous L-type donors. The reaction mechanism was experimentally and theoretically investigated to probe the origin of the observed selectivity switch.

# RESULTS AND DISCUSSION

## Low-Coordinate Co(I) Complex (IPr)Co[N(SiMe<sub>3</sub>)DIPP]

(2). Given our previous report of the two-coordinate iron complex (IPr)Fe[N(SiMe<sub>3</sub>)DIPP] and its catalytic efficacy in alkyne trimerization, it was of interest to prepare the cobalt congener and examine its potential catalytic properties. <sup>27,29,30</sup> Synthesis of the heteroleptic two-coordinate Co<sup>I</sup> complex follows the one-pot reaction sequence used to prepare the analogous Fe complex. <sup>27</sup> The Co<sup>II</sup> bis(amido) species Co[N(SiMe<sub>3</sub>)DIPP]<sub>2</sub> (1), prepared according to the literature

Figure 2. Structurally characterized cobalt diazoalkane adducts (relevant bond lengths and angles noted in blue and red, respectively). 37-39,48-51

procedure,<sup>31</sup> was treated with one equiv of NEt<sub>3</sub>·HCl in tetrahydrofuran (THF) at ambient temperature (25 °C). Next, a THF solution of 1 equiv of IPr was added dropwise to the same reaction mixture, followed by 1.05 equiv of KC<sub>8</sub> at -30 °C, resulting in a dark yellow solution (Scheme 1). Workup and crystallization from a hexamethyldisiloxane/toluene solution gave plate-shaped yellow-orange crystals in 73% yield. Single-crystal X-ray diffraction analysis revealed the product as (IPr)Co[N(SiMe<sub>3</sub>)DIPP] (2, Figure 1a), which exhibits Co-N and Co-C bond lengths of 1.863(5) and 1.936(6) Å, respectively, similar to those reported for (IPr)Co[N(SiMe<sub>3</sub>)<sub>2</sub>].<sup>30</sup> The bond lengths are slightly shorter than those reported for the analogous Fe complex<sup>27</sup> and slightly longer than those for the Ni analogue.<sup>32</sup> A presumed reaction mechanism for the formation of 2 is given in Scheme 1

Compound **2** is indefinitely stable in the solid state under nitrogen at ambient temperature, showing no sign of decomposition by  $^1$ H NMR spectroscopy after several months. Analysis of **2** by the Evans method<sup>33</sup> led to a surprisingly high magnetic moment of 4.8  $\mu_{\rm B}$ , which is significantly larger than the expected spin-only value of 2.8  $\mu_{\rm B}$  for a high-spin  $d^8$  electronic configuration. This enhanced moment is attributable to spin—orbit coupling frequently seen in open-shell two-coordinate complexes and has been observed for linear cobalt species,  $^{34,35}$  though interestingly, not for the isoelectronic Ni<sup>II</sup> species Ni[N(SiMe<sub>3</sub>)(DIPP)]<sub>2</sub> with a similar coordination geometry (2.67  $\mu_{\rm B}$ ).  $^{25}$ 

Isolation and Electronic Structure Characterization of a Diazoalkane Adduct. With a well-characterized, low-valent cobalt species in hand, its reducing character toward unsaturated organic molecules was investigated. Diazoalkanes are of interest as substrates known to exhibit divergent reactivity with cobalt complexes. Binding of the terminal N atom to cobalt leads to the formation of reduced ligand species such as the  $\beta$ -diketiminate-supported Co<sup>II</sup> diazoalkane radical anion complex (LCo(N<sub>2</sub>CPh<sub>2</sub>), L = {[(Dipp)-NC<sup>t</sup>Bu]<sub>2</sub>CH}<sup>-</sup>), whereas interaction of cobalt with the diazo-C atom can result in N<sub>2</sub> expulsion 40-42 to form the carbene complex as in Co(OR)<sub>2</sub>(CPh<sub>2</sub>) (R = CPh(<sup>t</sup>Bu)<sub>2</sub>). 40,43

Slow addition of 1 equiv of FluN<sub>2</sub> to 2 in Et<sub>2</sub>O by dropwise addition at ambient temperature resulted in an immediate color change from light yellow to dark orange. Plate-like dark

orange crystals were obtained in 81% yield after workup, and X-ray crystallography revealed this product to be the terminal diazoalkane adduct (IPr)Co[N(SiMe<sub>3</sub>)DIPP](N<sub>2</sub>Flu) (3). The Co center exists in an approximate trigonal planar geometry (Figure 1b,  $\sum \angle @$ Co = 359.9°). The diazo fragment displays significant bending  $[\angle N_{diazo} - N_{diazo} - C = 140.1(6)^{\circ}]$ with elongation of the  $N_{diazo}-N_{diazo}$  bond (1.216(6) Å) and a  $N_{diazo}-C$  bond length of 1.304(7) Å. For comparison, free FluN<sub>2</sub> exhibits analogous bond lengths of 1.126(4) and 1.324(4) Å in the solid state, respectively.<sup>44</sup> Depending on the bond metrics, diazoalkane ligands can be classified as neutral, dianionic (hydrazonido), or more rarely, monoanionic (a radical anion), and these electronic structures dictate available reaction pathways (e.g., involving C-N or N-N bond cleavage). 38,39,45 In this context, low-coordinate cobalt diazoalkane adducts should be particularly interesting, given their tendency toward high-spin configurations with unpaired electron density due to low ligand field strength. 38,39 The geometry of 3 closely resembles that observed by Holland and co-workers in 4 (Figure 2), suggesting a similar single-electron reduction of the diazo fragment and radical anion character for the FluN<sub>2</sub> ligand (Figure 1c). 39,46

To further probe the frontier molecular orbital structure of diazoalkane adduct 3, density functional theory (DFT) calculations were carried out starting from coordinates for the solid-state structure (see Supporting Information for the Computational Details). Our computational results indicated that 3 features a triplet ground state (Table S15) and is spincontaminated with an expectation value of the electron spin angular momentum  $\langle S^2 \rangle$  of 2.75. The computed bond lengths are in good agreement with the experimental values. For example, the Co-N<sub>diazo</sub> bond distance was calculated as 1.86 Å (1.793(5) Å from the experiment), while the  $N_{diazo}-N_{diazo}$  and N<sub>diazo</sub>-C bond distances were 1.22 and 1.31 Å, respectively (1.216(6) and 1.304(7) Å from the experiment). Moreover, the  $\angle Co-N_{diazo}-N_{diazo}$  and  $\angle N_{diazo}-N_{diazo}-C$  bond angles are computed to be 149.0 and 135.4°, respectively, consistent with the X-ray crystallographic structure of 3 (Figure 2) and the presence of diazoalkane radical anion character. Thus, the maximally paired electrons for the  $\alpha$ - and  $\beta$ -spin manifolds were computed. These indicated an overlap integral of 0.55, similar to the value reported by Holland and co-workers (cf. 0.67, Figure S7).<sup>39</sup> Furthermore, both the Mulliken spin

#### Scheme 2

Table 1. Effect of L-Type Donor on the Product Distribution

$$\begin{array}{c} N_2 \\ X \text{ equiv L-type donor} \\ \hline C_6D_6 \\ 25 \text{ °C} \\ \end{array}$$

L-type donor	amount	ratio of 8:9 <sup>a</sup>
none <sup>b</sup>	N/A	11:89
$THF^c$	solvent	100:0
cyclopentene <sup>b</sup>	1 equiv	11:89
$N_iN$ -dimethylallylamine $^b$	1 equiv	50:50
<i>tert-</i> butylnitrile <sup>b</sup>	1 equiv	75:25

<sup>a</sup>Product ratio determined by <sup>1</sup>H NMR analysis. <sup>b</sup>C<sub>6</sub>D<sub>6</sub> used as reaction solvent. <sup>c</sup>THF used as reaction solvent.

population on cobalt ( $\rho_{\text{Co}} = 2.53$ , Figure 1c) and the localized orbital bonding analysis (LOBA) imply that the cobalt center is in a formal +2 oxidation state (Figure S8). Based on the experimental and computational data, we proposed that 3 is best described as a high-spin divalent cobalt center that is antiferromagnetically coupled to one unpaired electron on the diazoalkane fragment, yielding an overall triplet spin ground state (S = 1, Figure 1c). Indeed, analysis of 3 by the Evans method led to a magnetic moment of 2.5  $\mu_{\text{B}}$ , in good agreement with the spin-only magnetic moment of 2.8  $\mu_{\text{B}}$  for triplet systems. Accordingly, all calculations in this study have been performed on the triplet potential energy surface.

Catalytic Diazoalkane Coupling Reaction Using **Complexes 2 and 3.** Compound 3 is thermally stable in benzene-d<sub>6</sub> at 80 °C for at least 16 h; however, dropwise treatment of 3 with one additional equivalent of FluN2 in benzene- $d_6$  under ambient conditions led to the vigorous evolution of a gas. The <sup>1</sup>H NMR spectrum taken after the bubbling had ceased showed complete conversion of FluN<sub>2</sub> and the formation of the corresponding hydrazine (8) and alkene (9) products in 11 and 89% yields, respectively, without any consumption of diazoalkane adduct 3 (Scheme 2). This stoichiometric reaction suggested that the homocouplings of FluN<sub>2</sub> to generate 8 and 9 could be catalyzed by either 2 or 3, and 3 is more thermodynamically favorable to catalytic turnover to regenerate 2. Indeed, treatment of 2 with 50 equiv of FluN<sub>2</sub> in benzene- $d_6$  at ambient temperature led to an instantaneous color change to dark orange (3) along with strong effervescence. Monitoring the reaction by <sup>1</sup>H NMR spectroscopy showed full consumption of FluN2 over 3 h, resulting in the formation of 8 and 9 in 11 and 89% yield, respectively (by <sup>1</sup>H NMR spectroscopy), along with the generation of 3.

Given the favored production of olefin 9 compared to hydrazine 8 in benzene- $d_6$ , the effects of the solvent on the product distribution were investigated. Interestingly, in THF, the catalysis also led to full conversion of FluN<sub>2</sub> in 3 h under ambient conditions. Analysis of the resulting product mixture by <sup>1</sup>H NMR spectroscopy surprisingly revealed the exclusive and quantitative formation of hydrazine 8, in contrast to the result obtained from benzene- $d_6$ . We considered two potential explanations for the observed solvent effect: (1) a more polar reaction medium (THF) provides greater stabilization for more polar transition states or intermediates to reverse the energetic preference for 8 vs 9, <sup>6,17</sup> and/or (2) coordination of THF to the cobalt center alters the electronic structure and primary coordination environment of a key intermediate, leading to a switch in product selectivity. <sup>28,35</sup>

To probe the possible effects derived from changes in the metal coordination sphere, the catalysis was monitored in benzene- $d_6$  in the presence of various equimolar amounts of exogenous L-type donors (Table 1). While the presence of a weak donor such as cyclopentene did not influence the reaction outcome, significant effects were observed for stronger ligands such as  $N_iN$ -dimethylallylamine and tert-butylnitrile, leading to 8/9 ratios of 1:1 and 3:1, respectively. These results suggest that the coordinating ability of good L-type donors such as organonitriles contributes to the observed selectivity switch.

Mechanism of Diazoalkane Coupling Catalysis. To elucidate the mechanism of this homocoupling transformation and shed light on the underlying principles responsible for the observed switch in product distribution, the kinetics of this catalytic transformation was probed both experimentally via <sup>1</sup>H NMR kinetics and theoretically using DFT calculations. To establish the dependence of the rate on FluN<sub>2</sub> concentration, 14.3 equiv of FluN<sub>2</sub> was combined with 2 in 1 mL of benzene-

 $d_6$  (7 mol % catalyst loading), and the concentration of FluN<sub>2</sub> was monitored by  $^1$ H NMR spectroscopy. A linear relationship was obtained for the natural log of substrate consumption over time (Figure 3), indicating a first-order dependence of the

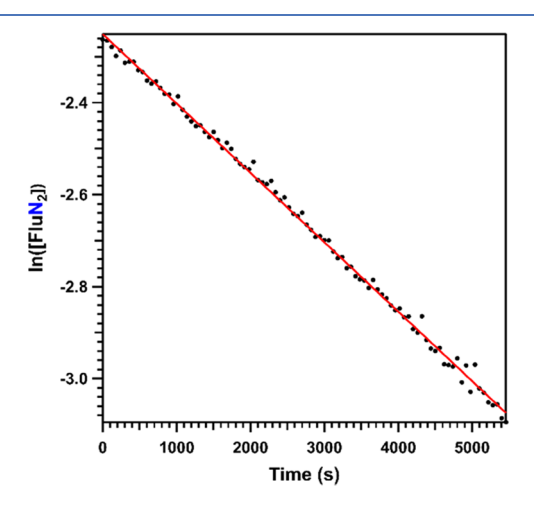


**Figure 3.** Natural log plot for  $FluN_2$  consumption (0.10 M) using 6.9 mol % of **2.** The red solid line represents a linear fit of  $ln([FluN_2])$  over time ( $R^2 = 0.997$ ) used to extract observed rate constants ( $k_{obs}$ ).

reaction rate on  $FluN_2$  concentration.<sup>53</sup> To determine the reaction order in catalyst 2, similar experiments were carried out using various catalyst concentrations from 2.8 to 14 mol %. Plotting the  $k_{\rm obs}$  values obtained from each run versus catalyst loading revealed a linear relationship (Figure 4), reflecting a

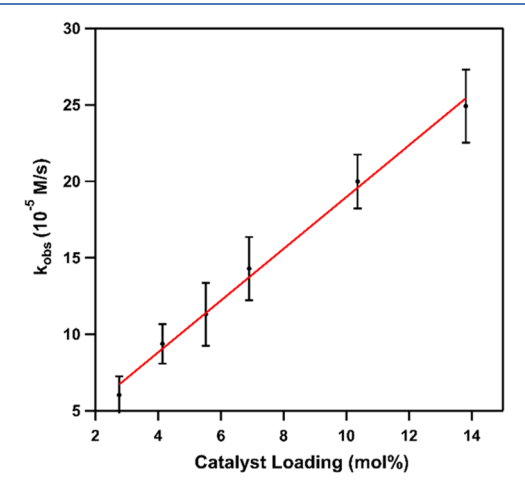


**Figure 4.** Observed rate constants  $(k_{\text{obs}})$  as a function of catalyst loadings (2) with every measurement done in triplicate. Error bars represent standard deviations. The red solid line represents a linear fit of  $k_{\text{obs}}$  over catalyst loading  $(R^2 = 0.995)$ .

first-order dependence of the reaction rate on catalyst concentration. Sa Each kinetic experiment was reproduced in triplicate, and error bars were plotted using the standard deviations. The H NMR spectra during each catalytic run indicated complete conversion of 2 into diazoalkane adduct 3 at the beginning of the catalysis, and the product ratios between 8 and 9 were consistent across all kinetic runs. Furthermore, analysis of the spectra indicated that no additional catalytic intermediates (other than 3) were observed during the catalysis. Thus, we concluded that 3 is the resting state of the catalyst during the transformation.

With the establishment of the experimentally determined rate law, we sought to use theory to study the elementary steps leading to the two products and pinpoint the origin of the observed selectivity switch. Therefore, the reaction pathways giving rise to 8 and 9 were simulated in the nonpolar medium benzene ( $\varepsilon=2.2706$ ) and in the polar environment with THF solvent ( $\varepsilon=7.4257$ ), in the absence of any solvent coordination to solely examine the role of solvent polarity. Sequentially, the same pathways were modeled with exogenous L-type donors, such as THF and acetonitrile, bound to the cobalt center to probe the effects derived from changes in the metal coordination sphere. Note that all Gibbs free energies ( $\Delta G$ ) reflect the relative differences with respect to the separated catalyst 2 and FluN<sub>2</sub>.

To simulate the conversion of FluN<sub>2</sub> to 8 and 9 in benzene, the initial formation of the resting state 3 was first calculated. This process is energetically downhill by 5.9 kcal/mol relative to the separated reactants, consistent with experimental data. Since the reaction is first order in FluN<sub>2</sub> concentration, another molecule of FluN<sub>2</sub> was brought into the calculation. Coordination of the second FluN<sub>2</sub> to cobalt is approximately thermoneutral ( $\Delta G = -5.3$  kcal/mol, not shown here). However, an exhaustive search for reaction pathways following the binding of a second FluN<sub>2</sub> did not yield any energetically reasonable mechanism for product generation. Therefore, a direct attack of a second FluN<sub>2</sub> onto the metal-bound diazoalkane fragment in 3 was investigated to determine the possibility of C–N and N–N bond-forming processes that generate products 8 and 9.

As shown in Figure 5, a plausible mechanism for the formation of hydrazine 8 involves electrophilic attack (vide infra) of the terminal nitrogen atom of the exogenous FluN2 onto the diazo carbon atom of the coordinated FluN2 in 3. In the associated transition state for this process, TS(3-10), the external FluN<sub>2</sub> approaches the bound hydrazine catalyst to a N…C distance of 1.89 Å with simultaneous N–C bond cleavage in the coordinated FluN<sub>2</sub> (N···C = 1.38 Å; Figure 5). This process continues with the production of 8, and the nitrogen atoms associated with the starting diazoalkane ligand remain in the cobalt's coordination sphere to give the dinitrogen complex 10. This elementary step corresponds to the TOF-determining transition state of the coupling reaction  $(\Delta G^{\ddagger} = 20.2 \text{ kcal/mol}, X_{\text{TOF}} = 1.00, \text{ Table S3}).$  Finally, complex 10 undergoes N2 expulsion to regenerate catalyst 2 (Figure 5).

Despite the straightforward pathway by which hydrazine 8 was formed in this catalysis, identifying a mechanism for forming the C=C bond in olefin 9 was more complicated. Following the investigation of various attack modes for exogenous FluN<sub>2</sub> onto 3, the most kinetically plausible transition state was identified as yielding an N-N bond between the two terminal N-atoms in both FluN<sub>2</sub> (TS(3-11), Figure 6). The ease for an N-N coupling event likely results from the ligand-based radical character of 3 as indicated by the Mulliken spin population in TS(3-11) (Figure S12). Isomerization around the N-N bond in 11 shortens the distance between the two diazo carbon atoms (12, d(C-C) = 2.74 Å), priming them for C-C bond formation. The subsequent C-C coupling event generates a cobalt-bound 1,2,3,4-tetrazine intermediate 13 ( $\Delta G = -3.4 \text{ kcal/mol}$ ), from which a ringopening, followed by N2 liberation, yields the olefin 9 and catalyst 2. Overall, ring-opening of the tetrazine fragment is the TOF-determining transition state (TS(13-14),  $\Delta G^{\ddagger} = 16.9$ 

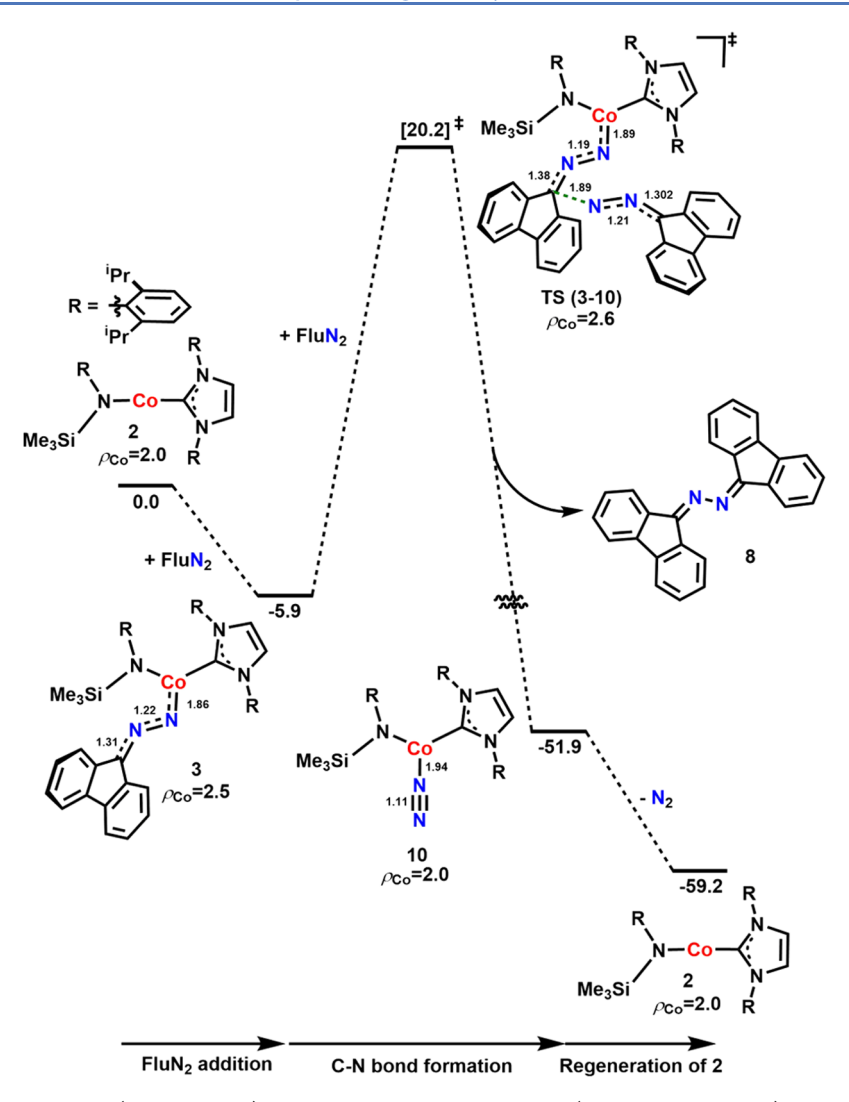


Figure 5. Computed Gibbs free energy ( $\Delta G$ , kcal/mol) profile for the formation of 1,2-di(9*H*-fluoren-9-ylidene)hydrazine (8) in the presence of 2 and FluN<sub>2</sub>. All free energies were calculated with respect to separated reactants (2, FluN<sub>2</sub>), and all complexes have a triplet ground state. The spin on cobalt is denoted as  $\rho_{Co}$ , and key distances are noted in angstroms (Å).

kcal/mol,  $X_{\text{TOF}} = 0.81$ , Table S5), although both the attack of exogenous FluN<sub>2</sub> ( $\Delta\Delta G^{\ddagger} = -0.5 \text{ kcal/mol}$ ) and C-C bond formation ( $\Delta \Delta G^{\ddagger} = -0.9 \text{ kcal/mol}$ ) have similar activation barriers. Note that the regenerated catalyst 2 in both of the previously mentioned mechanisms is expected to quickly convert into the resting state 3, which, as previously described, is downhill by 5.9 kcal/mol (Figures 5 and 6). It is worth mentioning that the cobalt center retains its spin density during the transformation from 3 until the release of the olefin 9 with a doublet formulation of the coupled FluN<sub>2</sub> fragment throughout. The open-shell nature of the FluN, ligand likely plays a crucial role in facilitating the N-N (TS(3-11)) and C-C (TS(12-13)) coupling event as well as the breakdown of the tetrazine intermediate (TS(13-14)), as shown by the Mulliken spin populations (Figures S12–S14), highlighting the importance of single-electron transformations involved in firstrow transition metal catalysis.

Based on the computed Gibbs free energy profiles for the formations of **8** (Figure 5) and **9** (Figure 6) in benzene, the energy span model (ESM) proposed by Kozuch and coworkers was adopted to calculate the overall reaction rate producing the two products.  $^{54,55}$  Interestingly, the TOF for yielding **8** is predicted as  $4.6 \times 10^{-7}$  s<sup>-1</sup> (Table S2), while the

TOF for 9 is  $2.3 \times 10^{-6}$  s<sup>-1</sup> (Table S4), in good agreement with the observed preference for product 9 formation in a nonpolar medium.

To understand the effect of solvent polarity on product distribution, the same calculations were carried out in polar solvent THF utilizing its dielectric constant and refractive index. The result, gratifyingly, confirmed a lowered barrier for production of 8 (TS(3–10),  $\Delta G_{\text{THF}}^{\ddagger} = 16.4$  kcal/mol, Table 2) with a predicted TOF of 2.6  $\times$  10<sup>-5</sup> s<sup>-1</sup> (Table S10), in contrast to a relatively slower generation of 9 (TOF =  $6.4 \times$  $10^{-6}$  s<sup>-1</sup>, Table S12). Given that the solvent model was the only difference between the calculations carried out in benzene and THF, the preferential generation of 8 in a more polar medium is proposed to result from solvent stabilization of the reaction pathway consisting of transition states with higher polarities. Indeed, the theoretically modeled electric dipole moment for the rate-limiting C-N bond-forming transition state in the production of 8 (10.37 D, TS(3-10), Table 2) is significantly higher than those of the transition states leading to olefin 9 (6.44-8.40 D, Table 2), verifying that the preference for hydrazine 8 generation in THF can be attributed to a solvent stabilization effect.

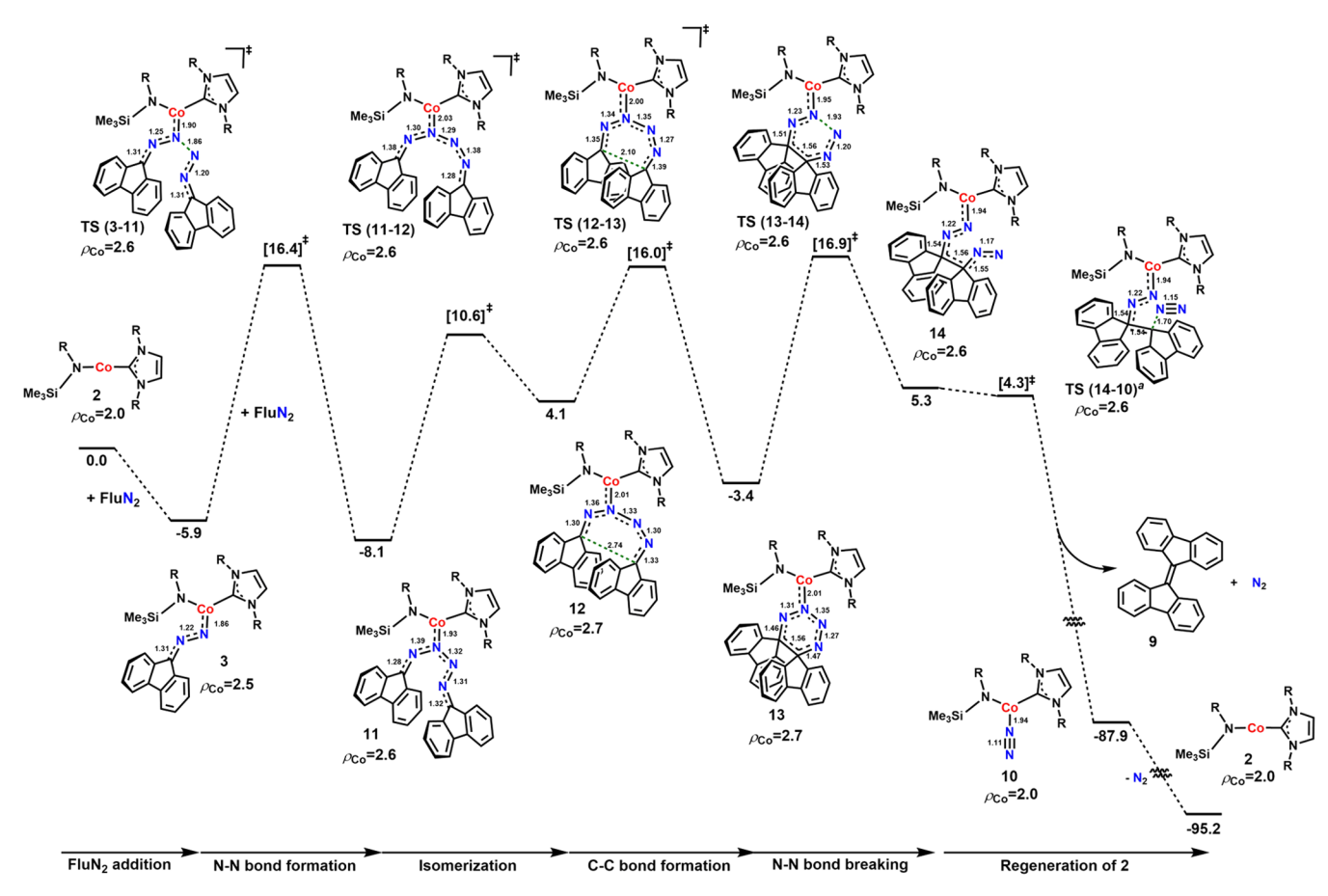


Figure 6. Computed Gibbs free energy ( $\Delta G$ , kcal/mol) profile for the formation of 9,9'-bifluorenylidene (9) in the presence of 2 and FluN<sub>2</sub>. All free energies are calculated with respect to the separated reactants, and all complexes have a triplet ground state. The spin on cobalt is denoted as  $\rho_{\text{Co}}$ , and key distances are noted in angstroms (Å). The forward reaction from 14 to 10 appears to be barrierless, as the transition state TS (14-10) has a lower zero-point energy than 14, offsetting the higher potential energy of the transition state with respect to the intermediate.

Table 2. Electric Dipole Moment (D) and Free Energy (kcal/mol) of Computed Intermediates and Transition States in the Generation of Hydrazine 8 and Olefin 9

computed species	electric dipole $moment^a(D)$	$\Delta G$ (kcal/mol) in benzene	$\Delta G$ (kcal/mol) in THF		
(A) Hydrazine 8 Generation					
2	9.17	0.0	0.0		
3	7.54	-5.9	-7.3		
TS (3-10)	10.37	20.2	16.4		
10	7.47	-51.9	-51.5		
(B) Olefin 9 Generation					
TS (3-11)	8.21	16.4	13.9		
11	5.98	-8.1	-10.4		
TS (11-12)	8.40	10.6	7.6		
12	6.79	4.1	1.1		
TS (12-13)	6.73	16.0	13.2		
13	6.54	-3.4	-6.3		
TS (13-14)	6.44	16.9	14.0		
<sup>a</sup> Calculated in the gas phase.					

Next, we studied the potential effect of L-type ligand coordination on product selectivity. A DFT model with THF bound to the cobalt center was constructed, initially following the same transformation pathways for both the generation of 8 and 9. The resulting potential energy surface, however, showed reversible binding of THF and increased kinetic barriers toward both the olefin and hydrazine products, with transition

state energies for C–N [TS(3–10), for 8] and N–N [TS(3–11), for 9] bond formation being increased from 16.4 and 13.9 kcal/mol to 25.6 and 26.4 kcal/mol, respectively. Since the spin density localized on the cobalt center remains constant throughout the reaction pathway, both in the presence and absence of bound THF, the increase in energy landscape is likely due to the escalated steric strain that resulted from the additional ligand. Therefore, the conversion of FluN<sub>2</sub> to 8 and 9 in THF likely does not involve THF coordination, and the selectivity switch entirely results from dipole—dipole stabilization of the more polar transition states.

Nonetheless, the altered product distribution in the presence of stronger L-type donors such as *tert*-butylnitrile propelled us to incorporate acetonitrile into our DFT model as an exogenous ligand that imposes an increased ligand field strength. Similarly, the corresponding energetics for the formation of alkene **9** in the presence of CH<sub>3</sub>CN is more disfavored, with the barrier for the TOF-determining tetrazine ring-opening transition state increased to  $\Delta G^{\ddagger} = 23.2$  kcal/mol (Figure S9), resulting in a much slower predicted TOF of 2.9  $\times$  10<sup>-9</sup> s<sup>-1</sup> (Table S8). Overall, we conclude that the CH<sub>3</sub>CN coordination is unlikely to alter the reaction energetics to produce olefin **9**, as in the case of THF coordination, as discussed above.

However, the coordination of acetonitrile to the cobalt center does accelerate the formation of hydrazine 8, as described in Figure 7. In this case, the TOF-determining

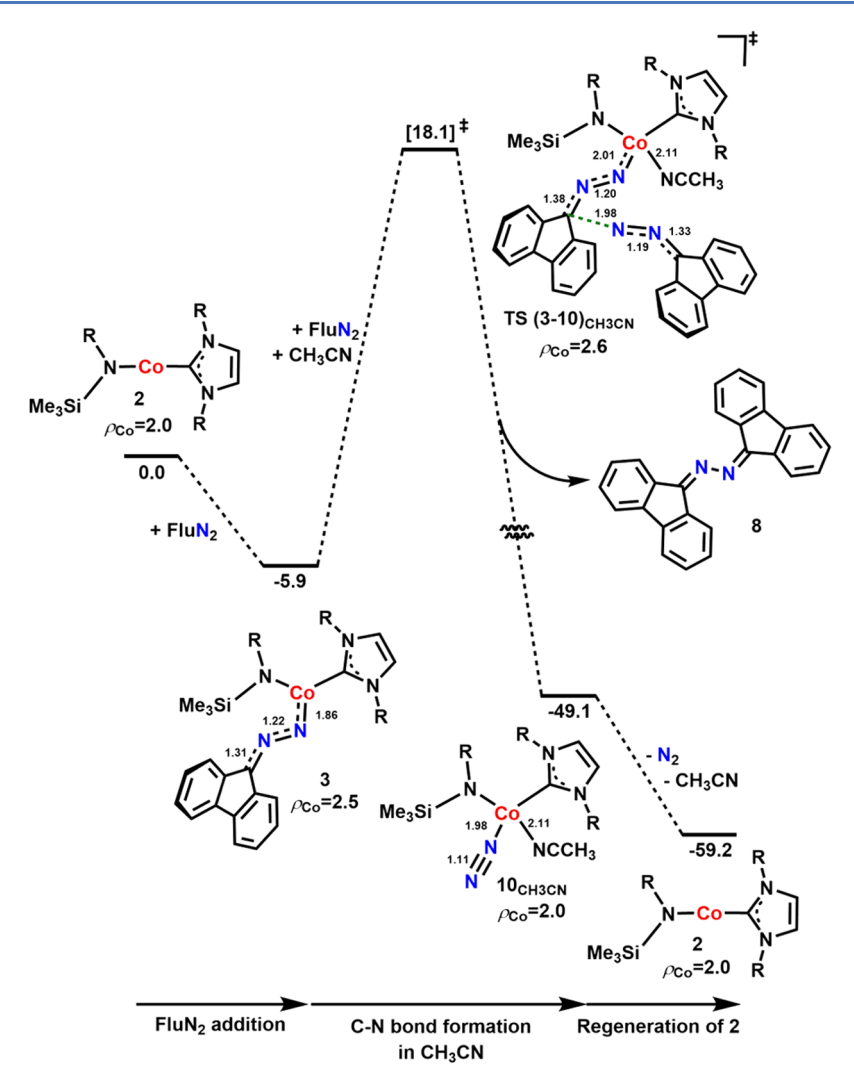


Figure 7. Computed Gibbs free energy ( $\Delta G$ , kcal/mol) profile for the formation of 1,2-di(9*H*-fluoren-9-ylidene)hydrazine (8) in the presence of 2, FluN<sub>2</sub>, and CH<sub>3</sub>CN. All free energies are calculated with respect to the separated reactants (2, FluN<sub>2</sub>, CH<sub>3</sub>CN), and all complexes have a triplet ground state. The spin on cobalt is denoted as  $\rho_{Co}$ , and key distances are noted in angstroms (Å).

transition state for C-N bond formation is lowered to 18.1 kcal/mol compared to that in the absence of any L-type donor  $(\Delta G^{\ddagger} = 20.2 \text{ kcal/mol}, \text{ Figure 5})$ . More interestingly, the TOF for forming 8, in this case, is calculated to be  $1.6 \times 10^{-5}$  s<sup>-1</sup> (Table S6), surpassing that for the formation of alkene 9 (TOF =  $2.3 \times 10^{-6}$  s<sup>-1</sup>, Table S4). Accordingly, this model predicts that good L-type donors (such as N,N-dimethylallylamine and tert-butylnitrile) assist the hydrazine formation, consistent with the observed switch in product selectivity (Table 1). Thus, the lowered barrier may, in principle, be attributed to increased steric strain in the coordination sphere and/or the altered ligand field electronic structure. However, since the attack of exogenous FluN<sub>2</sub> takes place on the remote diazo carbon atom of the FluN<sub>2</sub> fragment in 3, there is minimal steric interaction between the coordinated CH<sub>3</sub>CN and incoming FluN<sub>2</sub> (Figure \$10). Thus, the additional steric strain resulting from CH<sub>3</sub>CN coordination is unlikely the cause for the rate acceleration.

A detailed molecular orbital analysis was carried out to examine the changes in electronic structure brought about by the coordination of acetonitrile (Figure 8). The diazo carbon atom ( $C_A$ , DFT optimized T.S., Figure 8) in 3 appears to be nucleophilic in nature and is represented by a doubly occupied, delocalized frontier orbital with contributions from carbon and

nitrogen atomic p orbitals, as well as the cobalt  $d_{xz}$  orbital (arphi)or  $\varphi_{\text{CH3CN}}$ , Figure 8). Therefore, the mechanism with 3 involves nucleophilic attack of arphi onto the  $\pi^*( ext{N-N})$  orbital (lowest unoccupied molecular orbital—LUMO) of the FluN<sub>2</sub> substrate leading to hydrazine formation (DFT optimized T.S., Figure 8). Significantly, the coordination of CH<sub>3</sub>CN to 3 leads to destabilization of the corresponding orbital in 3(NCMe) (the  $\varphi_{\mathrm{CH3CN}}$  orbital) as a consequence of contributions from cobalt-ligand  $\sigma^*$  interactions. The heightened energy of this nucleophilic center presumably results in a more energetically favorable overlap with the substrate  $\pi^*(N-N)$  orbital, giving rise to a faster catalytic rate for the formation of 8. We hypothesize that the unpaired spin density on the FluN<sub>2</sub> fragment in 3 is likely not involved in the C-N bond-forming process. Indeed, the spin density predominately resides in the xy plane (Figures 8 and S11), orthogonal to the xz plane involving this addition reaction.

#### CONCLUSIONS

In conclusion, a low-coordinate cobalt system has been developed for the catalytic homocoupling of a diazoalkane to the corresponding olefin and hydrazine coupled products, with olefin as the predominant product in benzene. Interestingly,

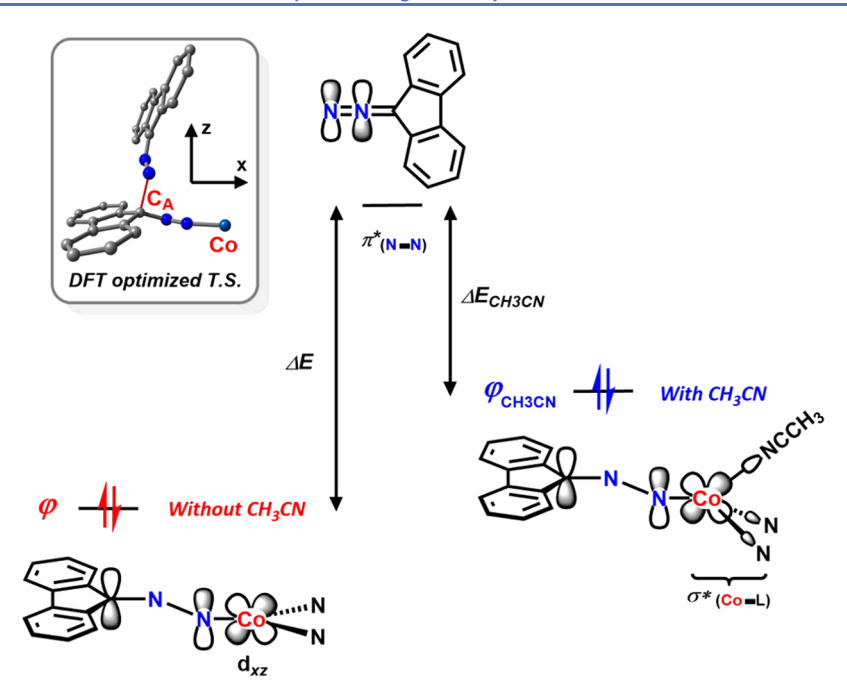


Figure 8. Molecular orbital analysis for the rate-determining C-N bond formation step in both the presence and absence of CH<sub>3</sub>CN [TS(3-10) and TS(3-10)<sub>CH3CN</sub>], showing a better energy match of  $\varphi_{\text{CH3CN}}$  than  $\varphi$  with the  $\pi^*(\text{N-N})$  orbital of exogenous FluN<sub>2</sub>.

the reaction selectivity switches in a polar medium, and this solvent effect derives from the stabilization of the more polar C–N bond-forming transition state. Additionally, the presence of a good L-type donor at cobalt renders the nitrogen-based diazenido ligand more electron-rich and accelerates a resulting nucleophilic attack of the metal complex onto the electrophilic substrate. The redox non-innocent nature of the FluN<sub>2</sub> ligand engenders a broken-symmetry formulation of the diazo complex as characterized by theoretical calculations. The open-shell electronic structure of the FluN<sub>2</sub> ligand facilitates a series of bond-forming and breaking events in the process of olefin generation, highlighting the importance of understanding electronic structures of reactive intermediates at deciphering the single-electron processes often associated with first-row transition metal catalysis.

# ASSOCIATED CONTENT

#### Supporting Information

The Supporting Information is available free of charge at https://pubs.acs.org/doi/10.1021/acscatal.1c02926.

Experimental procedures, characterization data for all new compounds, and computational results (PDF)

Cartesian coordinates for theoretical calculations (PDF)

X-ray crystallographic data for compound 2 (CIF)

X-ray crystallographic data for compound 3 (CIF)

# AUTHOR INFORMATION

## **Corresponding Authors**

Julien A. Panetier — Department of Chemistry, State
University of New York at Binghamton, Binghamton, New
York 13902, United States; orcid.org/0000-0003-49058396; Email: panetier@binghamton.edu

T. Don Tilley – Department of Chemistry, University of California, Berkeley, Berkeley, California 94720, United States; Chemical Sciences Division, Lawrence Berkeley National Laboratory, Berkeley, California 94720, United States; orcid.org/0000-0002-6671-9099; Email: tdtilley@berkeley.edu

#### **Authors**

Yuyang Dong — Department of Chemistry, University of California, Berkeley, Berkeley, California 94720, United States; Chemical Sciences Division, Lawrence Berkeley National Laboratory, Berkeley, California 94720, United States; Occid.org/0000-0002-4533-4798

Michael I. Lipschutz — Department of Chemistry, University of California, Berkeley, Berkeley, California 94720, United States; Chemical Sciences Division, Lawrence Berkeley National Laboratory, Berkeley, California 94720, United States

Ryan J. Witzke — Department of Chemistry, University of California, Berkeley, Berkeley, California 94720, United States; Chemical Sciences Division, Lawrence Berkeley National Laboratory, Berkeley, California 94720, United States; Occid.org/0000-0003-1729-1636

Complete contact information is available at: https://pubs.acs.org/10.1021/acscatal.1c02926

## **Author Contributions**

"Y.D. and M.I.L. contributed equally to this work.

#### Notes

The authors declare no competing financial interest.

#### ACKNOWLEDGMENTS

The work in Berkeley was funded by the NSF under Grant no. CHE-1954808. The authors acknowledge the National Institutes of Health (NIH) for funding the UC Berkeley CheXray X-ray crystallographic facility under Grant no. S10-RR027172, the UC Berkeley College of Chemistry NMR facility under Grant nos. SRR023679A, S10OD024998, and 1S10RR016634-01, and Beamline 11.3.1/12.2.1 of the Advanced Light Source, which is a DOE Office of Science User Facility under Contract no. DE-AC02-05CH11231.

Electronic structure calculations were performed on the Spiedie cluster at Binghamton University.

#### REFERENCES

- (1) Guo, C.; Fleige, M.; Janssen-Müller, D.; Daniliuc, C. G.; Glorius, F. Switchable selectivity in an NHC-catalysed dearomatizing annulation reaction. *Nat. Chem.* **2015**, *7*, 842.
- (2) Luo, K.; Zhang, L.; Jiang, H.; Chen, L.; Zhu, S. Selectivity-switchable construction of benzo-fused polycyclic compounds through a gold-catalyzed reaction of enyne-lactone. *Chem. Commun.* **2018**, *54*, 1893.
- (3) Masson-Makdissi, J.; Vandavasi, J. K.; Newman, S. G. Switchable Selectivity in the Pd-Catalyzed Alkylative Cross-Coupling of Esters. *Org. Lett.* **2018**, *20*, 4094.
- (4) Escorihuela, J.; Burguete, M. I.; Luis, S. V. New advances in dual stereocontrol for asymmetric reactions. *Chem. Soc. Rev.* **2013**, *42*, 5595.
- (5) Blanco, V.; Leigh, D. A.; Marcos, V. Artificial switchable catalysts. Chem. Soc. Rev. 2015, 44, 5341.
- (6) Sherwood, J.; Clark, J. H.; Fairlamb, I. J. S.; Slattery, J. M. Solvent effects in palladium catalysed cross-coupling reactions. *Green Chem.* **2019**, *21*, 2164.
- (7) Mulina, O. M.; Pirgach, D. A.; Nikishin, G. I.; Terent'ev, A. O. Switching of Sulfonylation Selectivity by Nature of Solvent and Temperature: The Reaction of  $\beta$ -Dicarbonyl Compounds with Sodium Sulfinates under the Action of Iron-Based Oxidants. *Eur. J. Org. Chem.* **2019**, 2019, 4179.
- (8) Dolewski, R. D.; Fricke, P. J.; McNally, A. Site-Selective Switching Strategies to Functionalize Polyazines. *J. Am. Chem. Soc.* **2018**. *140*. 8020.
- (9) Tang, H.; Tian, Y.-B.; Cui, H.; Li, R.-Z.; Zhang, X.; Niu, D. Siteswitchable mono-O-allylation of polyols. *Nat. Commum.* **2020**, *11*, No. 5681
- (10) Xin, F.; Rong, Y.; Fang, W.; Xu, Z.; Qing, X.; Lei, Y. Copper-Catalyzed Selectivity-Switchable Dehydration/Beckmann Rearrangement Reactions of Aldoxime. *Chin. J. Org. Chem.* **2018**, *38*, 2736.
- (11) Zhu, C.-Z.; Feng, J.-J.; Zhang, J. Divergent synthesis of functionalized pyrrolidines and  $\gamma$ -amino ketones via rhodium-catalyzed switchable reactions of vinyl aziridines and silyl enol ethers. *Chem. Commun.* **2018**, 54, 2401.
- (12) Cowley, R. E.; Eckert, N. A.; Vaddadi, S.; Figg, T. M.; Cundari, T. R.; Holland, P. L. Selectivity and Mechanism of Hydrogen Atom Transfer by an Isolable Imidoiron(III) Complex. *J. Am. Chem. Soc.* **2011**, *133*, 9796.
- (13) Baek, Y.; Betley, T. A. Catalytic C-H Amination Mediated by Dipyrrin Cobalt Imidos. J. Am. Chem. Soc. 2019, 141, 7797.
- (14) Proutiere, F.; Schoenebeck, F. Solvent Effect on Palladium-Catalyzed Cross-Coupling Reactions and Implications on the Active Catalytic Species. *Angew. Chem., Int. Ed.* **2011**, *50*, 8192.
- (15) Reeves, E. K.; Bauman, O. R.; Mitchem, G. B.; Neufeldt, S. R. Solvent Effects on the Selectivity of Palladium-Catalyzed Suzuki-Miyaura Couplings. *Isr. J. Chem.* **2020**, *60*, 406.
- (16) Schoenebeck, F.; Houk, K. N. Ligand-Controlled Regioselectivity in Palladium-Catalyzed Cross Coupling Reactions. *J. Am. Chem. Soc.* **2010**, *132*, 2496.
- (17) Hatanaka, Y.; Hiyama, T. Stereochemistry of the cross-coupling reaction of chiral alkylsilanes with aryl triflates: a novel approach to optically active compounds. *J. Am. Chem. Soc.* **1990**, *112*, 7793.
- (18) Grimster, N. P.; Gauntlett, C.; Godfrey, C. R. A.; Gaunt, M. J. Palladium-Catalyzed Intermolecular Alkenylation of Indoles by Solvent-Controlled Regioselective C-H Functionalization. *Angew. Chem., Int. Ed.* **2005**, 44, 3125.
- (19) Holland, P. L. Distinctive Reaction Pathways at Base Metals in High-Spin Organometallic Catalysts. Acc. Chem. Res. 2015, 48, 1696.
- (20) Bauer, I.; Knölker, H.-J. Iron Catalysis in Organic Synthesis. Chem. Rev. 2015, 115, 3170.
- (21) Cahiez, G.; Moyeux, A. Cobalt-Catalyzed Cross-Coupling Reactions. *Chem. Rev.* **2010**, *110*, 1435.

- (22) Vogiatzis, K. D.; Polynski, M. V.; Kirkland, J. K.; Townsend, J.; Hashemi, A.; Liu, C.; Pidko, E. A. Computational Approach to Molecular Catalysis by 3d Transition Metals: Challenges and Opportunities. *Chem. Rev.* **2019**, *119*, 2453.
- (23) Rana, S.; Biswas, J. P.; Paul, S.; Paik, A.; Maiti, D. Organic synthesis with the most abundant transition metal—iron: from rust to multitasking catalysts. *Chem. Soc. Rev.* **2021**, *50*, 243.
- (24) Miessler, G. L.; Fischer, P. J.; Tarr, D. A. Inorganic Chemistry, 5th ed.; Pearson, 2013.
- (25) Lipschutz, M. I.; Tilley, T. D. Synthesis and reactivity of a conveniently prepared two-coordinate bis(amido) nickel(II) complex. *Chem. Commun.* **2012**, *48*, 7146.
- (26) Lipschutz, M. I.; Tilley, T. D. Carbon—Carbon Cross-Coupling Reactions Catalyzed by a Two-Coordinate Nickel(II)—Bis(amido) Complex via Observable Ni<sup>I</sup>, Ni<sup>II</sup>, and Ni<sup>III</sup> Intermediates. *Angew. Chem., Int. Ed.* **2014**, 53, 7290.
- (27) Lipschutz, M. I.; Chantarojsiri, T.; Dong, Y.; Tilley, T. D. Synthesis, Characterization, and Alkyne Trimerization Catalysis of a Heteroleptic Two-Coordinate Fe<sup>I</sup> Complex. *J. Am. Chem. Soc.* **2015**, 137, 6366.
- (28) Lin, C.-Y.; Fettinger, J. C.; Power, P. P. Reversible Complexation of Lewis Bases to Low-Coordinate Fe(II), Co(II), and Ni(II) Amides: Influence of the Metal, Donor Ligand, and Amide Substituent on Binding Constants. *Inorg. Chem.* **2017**, *56*, 9892.
- (29) Liu, Y.; Deng, L. Mode of Activation of Cobalt(II) Amides for Catalytic Hydrosilylation of Alkenes with Tertiary Silanes. *J. Am. Chem. Soc.* **2017**, *139*, 1798.
- (30) Danopoulos, A. A.; Braunstein, P.; Monakhov, K. Y.; van Leusen, J.; Kögerler, P.; Clémancey, M.; Latour, J.-M.; Benayad, A.; Tromp, M.; Rezabal, E.; Frison, G. Heteroleptic, two-coordinate  $[M(NHC)\{N(SiMe_3)_2\}]$  (M = Co, Fe) complexes: synthesis, reactivity and magnetism rationalized by an unexpected metal oxidation state. *Dalton Trans.* **2017**, *46*, 1163.
- (31) Lin, C.-Y.; Guo, J.-D.; Fettinger, J. C.; Nagase, S.; Grandjean, F.; Long, G. J.; Chilton, N. F.; Power, P. P. Dispersion Force Stabilized Two-Coordinate Transition Metal—Amido Complexes of the  $-N(SiMe_3)Dipp$  (Dipp =  $C_6H_3$ -2,6- $Pr_2^i$ ) Ligand: Structural, Spectroscopic, Magnetic, and Computational Studies. *Inorg. Chem.* **2013**, *52*, 13584.
- (32) Lipschutz, M. I.; Tilley, T. D. Useful Method for the Preparation of Low-Coordinate Nickel(I) Complexes via Transformations of the Ni(I) Bis(amido) Complex  $K\{Ni[N(SiMe_3)(2,6-iPr_2-C_6H_3)]_2\}$ . Organometallics **2014**, 33, 5566.
- (33) Evans, D. F. 400. The determination of the paramagnetic susceptibility of substances in solution by nuclear magnetic resonance. *J. Chem. Soc.* **1959**, 2003.
- (34) Du, J.; Wang, L.; Xie, M.; Deng, L. A Two-Coordinate Cobalt(II) Imido Complex with NHC Ligation: Synthesis, Structure, and Reactivity. *Angew. Chem., Int. Ed.* **2015**, *54*, 12640.
- (35) Power, P. P. Stable Two-Coordinate, Open-Shell (d<sup>1</sup>-d<sup>9</sup>) Transition Metal Complexes. *Chem. Rev.* **2012**, *112*, 3482.
- (36) Mizobe, Y.; Ishii, Y.; Hidai, M. Synthesis and reactivities of diazoalkane complexes. *Coord. Chem. Rev.* **1995**, *139*, 281.
- (37) Dartiguenave, M.; Joëlle Menu, M.; Deydier, E.; Yves, D.; Siebald, H. Crystal and molecular structures of transition metal complexes with N- and C-bonded diazoalkane ligands. *Coord. Chem. Rev.* 1998, 178–180, 623.
- (38) Bonyhady, S. J.; DeRosha, D. E.; Vela, J.; Vinyard, D. J.; Cowley, R. E.; Mercado, B. Q.; Brennessel, W. W.; Holland, P. L. Iron and Cobalt Diazoalkane Complexes Supported by  $\beta$ -Diketiminate Ligands: A Synthetic, Spectroscopic, and Computational Investigation. *Inorg. Chem.* **2018**, *57*, 5959.
- (39) Bonyhady, S. J.; Goldberg, J. M.; Wedgwood, N.; Dugan, T. R.; Eklund, A. G.; Brennessel, W. W.; Holland, P. L. Cobalt(II) Complex of a Diazoalkane Radical Anion. *Inorg. Chem.* **2015**, *54*, 5148.
- (40) Bellow, J. A.; Stoian, S. A.; van Tol, J.; Ozarowski, A.; Lord, R. L.; Groysman, S. Synthesis and Characterization of a Stable High-Valent Cobalt Carbene Complex. *J. Am. Chem. Soc.* **2016**, *138*, 5531.

- (41) de Frémont, P.; Marion, N.; Nolan, S. P. Carbenes: Synthesis, properties, and organometallic chemistry. *Coord. Chem. Rev.* **2009**, 253, 862.
- (42) Mindiola, D. J.; Hillhouse, G. L. Synthesis, Structure, and Reactions of a Three-Coordinate Nickel-Carbene Complex, {1,2-Bis(di-tert-butylphosphino)ethane}NiCPh<sub>2</sub>. J. Am. Chem. Soc. 2002, 124, 9976
- (43) Grass, A.; Dewey, N. S.; Lord, R. L.; Groysman, S. Ketenimine Formation Catalyzed by a High-Valent Cobalt Carbene in Bulky Alkoxide Ligand Environment. *Organometallics* **2019**, *38*, 962.
- (44) Tulip, T. H.; Corfield, P. W. R.; Ibers, J. A. The crystal and molecular structure of 9-diazofluorene. *Acta Crystallogr., Sect. B: Struct. Sci.* **1978**, 34, 1549.
- (45) Reesbeck, M. E.; Grubel, K.; Kim, D.; Brennessel, W. W.; Mercado, B. Q.; Holland, P. L. Diazoalkanes in Low-Coordinate Iron Chemistry: Bimetallic Diazoalkyl and Alkylidene Complexes of Iron(II). *Inorg. Chem.* **2017**, *56*, 1019.
- (46) Neese, F. Definition of corresponding orbitals and the diradical character in broken symmetry DFT calculations on spin coupled systems. *J. Phys. Chem. Solids* **2004**, *65*, 781.
- (47) Chai, J.-D.; Head-Gordon, M. Long-range corrected hybrid density functionals with damped atom—atom dispersion corrections. *Phys. Chem. Phys.* **2008**, *10*, 6615.
- (48) Klein, H.-F.; Ellrich, K.; Hammerschmitt, B.; Koch, U.; Cordier, G. Koordination von Diazoverbindungen an Cobalt(I)-Zentren Struktur von Methyl(diazocyclopentadien)tris(trimethylphosphan)-cobalt. Z. Naturforsch. 1990, 45, 1291.
- (49) Jenkins, D. M.; Betley, T. A.; Peters, J. C. Oxidative Group Transfer to Co(I) Affords a Terminal Co(III) Imido Complex. *J. Am. Chem. Soc.* **2002**, *124*, 11238.
- (50) Ingleson, M. J.; Pink, M.; Caulton, K. G. Reducing Power of Three-Coordinate Cobalt(I). J. Am. Chem. Soc. 2006, 128, 4248.
- (51) Ingleson, M. J.; Pink, M.; Fan, H.; Caulton, K. G. Redox Chemistry of the Triplet Complex (PNP)Co<sup>I</sup>. J. Am. Chem. Soc. 2008, 130, 4262.
- (52) Cramer, C. J.; Truhlar, D. G. Implicit Solvation Models: Equilibria, Structure, Spectra, and Dynamics. *Chem. Rev.* **1999**, 99, 2161.
- (53) Anslyn, E. V.; Dougherty, D. A.; Dougherty, E. V.; Books, U. S. *Modern Physical Organic Chemistry*; University Science Books, 2006.
- (54) Kozuch, S.; Shaik, S. How to Conceptualize Catalytic Cycles? The Energetic Span Model. *Acc. Chem. Res.* **2011**, *44*, 101.
- (55) Uhe, A.; Kozuch, S.; Shaik, S. Automatic analysis of computed catalytic cycles. *J. Comput. Chem.* **2011**, 32, 978.